Reengineering orthogonally selective riboswitches

Neil Dixon[a,b], John N. Duncan[a,b], Torsten Geerlings[a,b], Mark S. Dunstan[b], John E. G. McCarthy[b], David Leys[b], and Jason Micklefield[a,b,1]

[a]School of Chemistry and [b]Manchester Interdisciplinary Biocentre, The University of Manchester, 131 Princess Street, Manchester M1 7DN, United Kingdom.

Edited by Dinshaw J. Patel, Memorial Sloan-Kettering Cancer Center, New York, NY, and approved December 22, 2009 (received for review September 29, 2009)

The ability to independently control the expression of multiple genes by addition of distinct small-molecule modulators has many applications from synthetic biology, functional genomics, pharmaceutical target validation, through to gene therapy. Riboswitches are relatively simple, small-molecule–dependent, protein-free, mRNA genetic switches that are attractive targets for reengineering in this context. Using a combination of chemical genetics and genetic selection, we have developed riboswitches that are selective for synthetic "nonnatural" small molecules and no longer respond to the natural intracellular ligands. The orthogonal selectivity of the riboswitches is also demonstrated in vitro using isothermal titration calorimetry and x-ray crystallography. The riboswitches allow highly responsive, dose-dependent, orthogonally selective, and dynamic control of gene expression in vivo. It is possible that this approach may be further developed to reengineer other natural riboswitches for application as small-molecule responsive genetic switches in both prokaryotes and eukaryotes.

synthetic biology | chemical genetics | gene regulation | RNA | aptamer

Riboswitches have been identified in all domains of life (1, 2), occurring with highest frequency within the 5′-UTRs of bacterial mRNAs, where they typically regulate genes involved in metabolite biosynthesis or transport (3). The bacterial riboswitches normally operate through the binding of a metabolite to an aptamer domain, which, through allosteric effects, changes the conformation of an adjacent expression platform resulting in either the premature termination of transcription, inhibition of translation initiation, or mRNA self-cleavage (3–6). In eukaryotes, riboswitches present within introns have also been shown to affect alternative splicing pathways (7). These simple protein-free mechanisms make the engineering of natural or synthetic riboswitches an attractive strategy for developing new small-molecule responsive regulatory systems (8).

In previous work synthetic riboswitches have been constructed using aptamers generated by in vitro selection. Notably, insertion of aptamers into the 5′-UTRs of bacterial or eukaryotic mRNAs (9–12), splice sites within introns of eukaryotic pre-mRNA (13, 14), or coupling of aptamers to ribozymes (15, 16) have shown significant potential for small-molecule modulation of gene expression. However, there are currently very few aptamers, generated by in vitro selection, that are selective for ligands with desirable physicochemical and pharmacokinetic properties (8). Moreover, in vitro selection approaches can be laborious (8), and it is not clear if some of the existing aptamers are completely selective for the desired ligand over structurally related molecules present within the cell. An alternative approach, which has been little explored to date, would be to reengineer existing natural riboswitches (17). A major problem with this approach is that the ligands for natural riboswitches are typically metabolites ordinarily present at varying levels in the cell, which severely limits their applicability as generic small-molecule responsive expression systems.

Here, we have applied a combination of chemical genetics and genetic selection to identify new riboswitches that allow orthogonally selective, tuneable, and dose-dependent control of gene expression in response to nonnatural synthetic small molecules. Our strategy involved mutagenesis of the aptamer domain of the adenine-sensing *add* A-riboswitch, found in the 5′-UTR of the adenine deaminase encoding gene of *Vibrio vulnificus* (4).

Results & Discussion

Selection of Mutant Riboswitches that Accept New Heterocyclic Ligands. The *add* A-riboswitch was chosen as the basis for this study because it functions at the translational level via a relatively simple mechanism that could potentially operate in any bacterial system (18, 19) (Fig. 1). Also, inexpensive or easily synthesised purine and other heterocyclic analogues, which possess desirable physicochemical properties, could potentially be used as ligands (20, 21). In previous studies, a number of other well-characterized purine riboswitches have also been identified. However, these function through modulation of transcription, by a more complex mechanism (22–25), which may be more organism-specific (26). From the x-ray crystal structures of the *add* A-riboswitch (18), it is clear that the aptamer domain entirely encapsulates adenine with four nucleotides (U22, U47, U51, and U74) making specific H-bonding contacts (Fig. 1*A* and *B*). The U74 nucleobase is believed to be the initial point of ligand recognition, through Watson–Crick base pairing, after which the loop J2/3 closes around the ligand, with additional contact to the 2′-OH of U22 through the purine N7 (18, 19, 25, 27).

Based on these structural insights, the nucleotides U47 and U51 of the *add* A-riboswitch (Fig. 1*B*) were chosen for mutagenesis. Accordingly, these nucleotides were fully randomized by site-directed mutagenesis to give all possible *add* A-riboswitch derivatives and cloned upstream of the chloramphenicol acetyl transferase (CAT) resistance gene under the control of the *lac* promoter in the pMOD3 vector (SI Text) (Fig. S1). The 15 mutant riboswitches were each screened for chloramphenicol resistance in the presence and absence of individual small molecules from a library of close to 80 heterocyclic analogues (Fig. S2). Mutant-ligand pairs identified by observing the number and size of colonies on agar plates with and without ligand were further assayed for antibiotic resistance in liquid medium using a 96-well plate reader (SI Text). Mutant riboswitch–ligand pairs that displayed significant differential growth rates that were dependent on small molecules from the library, but showed no change upon addition of adenine, were chosen for further characterization.

New Ligands Display No Cross-Activation of the Parent Riboswitch. The selected mutant riboswitches were cloned upstream of the eGFP gene in pMOD3 and the resulting *Escherichia coli* transformants were analyzed for eGFP expression upon addition of the putative ligand hits (SI Text). From this, a mutant

Author contributions: N.D., T.G., and J. Micklefield designed research; N.D. and J.N.D. performed research; T.G. contributed new reagents/analytic tools; N.D., J.N.D., T.G., J.E.G. McCarthy, and J. Micklefield analyzed data; N.D. and J. Micklefield wrote the paper; and M.S.D. and D.L. performed x-ray structure determination.

The authors declare no conflict of interest.

This article is a PNAS Direct Submission.

[1]To whom correspondence should be addressed. E-mail: Jason.micklefield@manchester.ac.uk.

This article contains supporting information online at www.pnas.org/cgi/content/full/0911209107/DCSupplemental.

www.pnas.org/cgi/doi/10.1073/pnas.0911209107

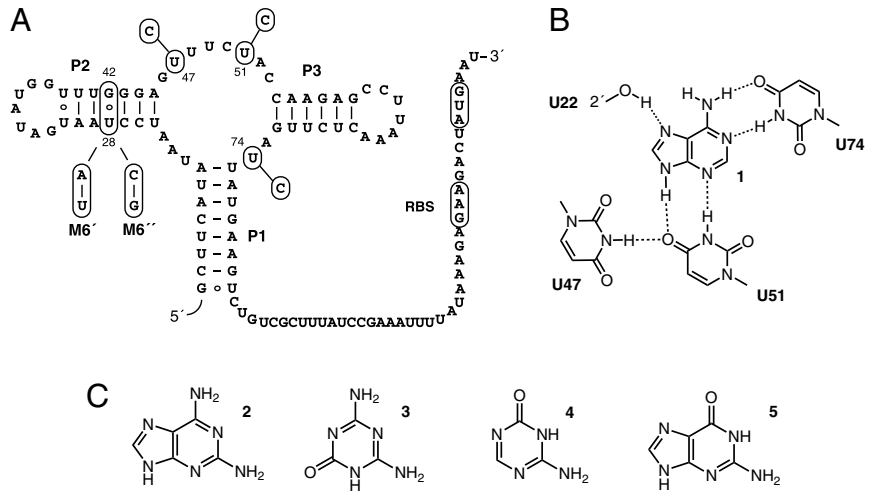

Fig. 1. (*A*) Secondary structure model of the parental *add* A-riboswitch in the ON-state when cognate ligand adenine **1** is bound and the ribosome binding site (RBS) is free. In the absence of adenine, an alternative structure (OFF-state) is formed, which sequesters the RBS and blocks translation. Bases circled indicate the mutations investigated in this study: M6 (U47C, U51C), M6C (U47C, U51C, U74C), M6′ (G42A, U47C, U51C), M6′′ (U28G, G42C, U47C, U51C), M6C′ (G42A, U47C, U51C, U74C), and M6C′′ (U28G, G42C, U47C, U51C, U74C). (*B*) The *add* A-riboswitch showing H-bonding contacts to the ligand adenine **1**. (*C*) The chemical structures of the ligands used in this study: adenine **1**, 2,6-diaminopurine **2**, ammeline **3**, azacytosine **4**, and guanine **5**.

riboswitch M6 (U47C, U51C), was shown to give an optimal response to ammeline **3** (Fig. 1*C*). The selected M6 riboswitch regulated eGFP expression dose-dependently over a broad dynamic range upon addition of ammeline **3** (Fig. 2*A*). The degree to which the M6 riboswitch controls gene expression, referred to as the induction factor, was determined from the ratio of the maximum ligand-induced protein expression over the basal protein expression level. For example, the mutant M6 exhibits a maximal induction factor of *circa* (*ca.*) 6.5 at a 500 μM dose of ammeline **3** (Fig. 2*A* and *B*). This compares with an induction factor of *ca.* 11 observed for the parental riboswitch upon addition of adenine **1** (500 μM). Ammeline **3** was further shown to have no effect upon eGFP expression under the control of the parental riboswitch, and most significantly adenine **1** had no effect upon eGFP expression under control of the mutant riboswitch M6 (Fig. 2*A*). These observations indicate that orthogonal control of gene expression is possible, simply by introducing two point mutations into the parent riboswitch aptamer domain. These mutations effectively block recognition of the natural ligand but allow the binding of the selected nonnatural ammeline ligand **3**, which in turn has no effect upon the parent riboswitch. These results are consistent with the earlier structural studies which show that nucleotides U47 and U51 confer selectivity within the purine riboswitches, by recognition of the N9-N3-N2 face of the purine ligand (Fig. 1*B*).

Given that the double mutant M6 (U47C, U51C) retains its functionality in vivo, we sought to explore further the structure-activity relationship by mutating U74 to cytosine to give the triple mutant M6C (U47C, U51C, U74C). Through Watson–Crick base pairing, U74 confers adenine versus guanine selectivity in the natural purine riboswitches (4, 25, 28) (Fig. 1). Despite this, the M6 and M6C mutants were surprisingly found to have partially overlapping ligand-response profiles, with the ammeline **3** also inducing eGFP expression with the M6C mutant albeit at a reduced induction factor of *ca.* 3.6 (Fig. 2*C*). The library of *ca.* 80 ligands (Fig. S2) was then screened against M6C-eGFP, and azacytosine **4** was identified, which displayed a similar induction factor of *ca.* 2.8 (Fig. 2*C*). Moreover, neither adenine **1** or guanine **5**, induce eGFP expression over the basal level, under the control of the M6C riboswitch. Also, azacytosine **4**, like ammeline **3**, has no effect on eGFP expression under control of the parental *add* A-riboswitch, demonstrating that the M6-**3** and M6C-**4** pairs both show orthogonal selectivities with respect to the parental riboswitch.

Mutations Within the P2 Stem Increase Absolute Reporter Gene Expression Levels. Significant induction factors were observed for M6 with ammeline **3** (of *ca.* 6.5), and for M6C with ammeline **3** (of *ca.* 3.6) and azacytosine **4** (of *ca.* 2.8). However, the maximum level of fluorescent protein produced per cell, as determined by comparing the normalized fluorescent units (fu/OD_{620}) at saturation (500 μM ligand), were 35–70% lower for the mutants in comparison to the parental switch (Fig. 2*B* and *C*). For example, riboswitches M6 and M6C both became saturated in the presence of ammeline **3** (500 μM) leading to maximum eGFP levels of *ca.* 3.4×10^6 and 6.7×10^6 fu/OD_{620}, respectively, whereas the parental riboswitch in the presence of adenine (500 μM) reached a maximum eGFP level of *ca.* 10.4×10^6 fu/OD_{620}. In order to improve the dynamic range of expression levels that can be accessed using these new riboswitch control elements, we first sought to subject M6 to further mutagenesis. Computational analysis using the mFold server (29) suggested that the mutations (U47C, U51C) introduced into the J2/3 loop result in a possible subpopulation of misfolded transcripts that would have a reduced ability to mediate translational regulation. C51 of the J2/3 loop of mutant M6 can potentially hybridize to G42 of a G-U wobble within the P2 stem (Fig. 1). To examine this misfolding hypothesis, mutants M6′ (G42A, U47C, U51C) and M6′′ (U28G, G42C, U47C, U51C) were prepared (SI Text). These mutants avoid possible misfolding caused by potential additional interactions between G42 and C51 and also strengthen the P2 stem through increased base pairing between nucleotides 28 and 42. The P2 stem mutations resulted in no significant change in the induction factor of 6.5 for the mutants M6, M6′, and M6′′ with ammeline **3** (Fig. 2*B*), as both the basal and ligand-induced levels of eGFP expression increased proportionally. Indeed, as the strength of nucleobase contacts between positions 28 and 42 increased (from U-G, U-A to G-C), so did the absolute maximal levels of eGFP expression (Fig. 2*B*). We rationalize these observations using a kinetic partitioning mechanism (30, 31), whereby increasing P2 stem strength increases the population of correctly folded riboswitches available to perform gene regulation, by minimizing the occurrence of the misfolded mRNA transcripts. As a consequence of increasing the P2 stem strength within the M6′ and M6′′

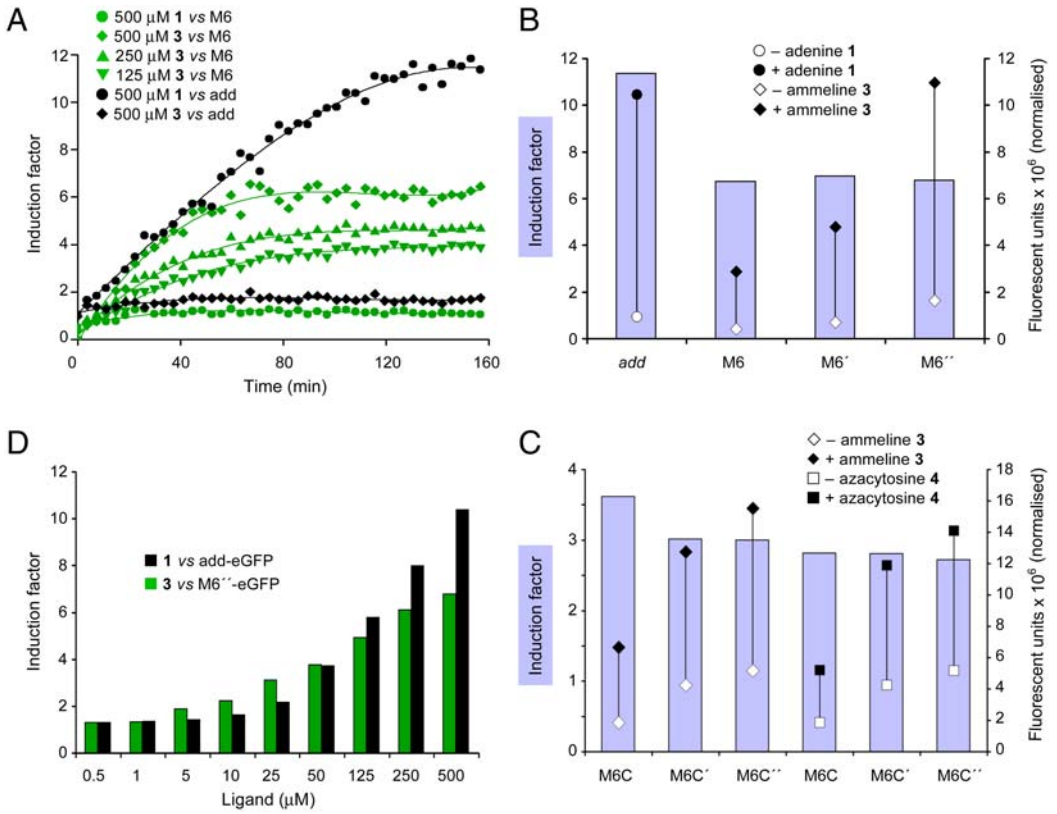

Fig. 2. (*A*) Ligand-dependent eGFP expression versus time under control of parental and M6 riboswitches: Parental riboswitch (*Black*) on addition of adenine **1** 500 μM (black circle) and ammeline **3** 500 μM (black diamond); M6 riboswitches (*Green*) in the presence of either ammeline **3** 500 μM (green diamond), 250 μM (green up triangle), 125 μM (green down triangle) and adenine **1** 500 μM (green circle). The eGFP fluorescence signal is normalized for cell density (fu/OD_{620}) and displayed as an induction factor, which is determined by taking the ratio of normalized eGFP signal in the presence and absence of ligand. (*B*) eGFP induction factors (left axis indicated by the gray bars) and absolute normalized eGFP fluorescence signal (right axis) in the absence of ligand (open shape) and in the presence of ligand (closed shape) for: parental *add* A-riboswitch in the presence of 500 μM adenine (black circle) and absence of adenine (open circle); M6, M6′, and M6′′ riboswitches in the presence of 500 μM ammeline **3** (black diamond), or absence of ammeline **3** (open diamond). (*C*) eGFP induction factors and absolute eGFP expression for M6C, M6C′, and M6C′′: in the presence of 500 μM ammeline **3** (black diamond), or absence of ammeline **3** (open diamond); in the presence of 500 μM azacytosine **4** (black square), or absence of azacytosine **4** (open square). (*D*) Dose-dependent eGFP expression under control of mutant M6′′ (green square) and parental *add* (black square) riboswitches showing induction factors over a range of ammeline **3** or adenine **1** ligand concentrations.

mutants, there also appears to be a change in the relative order of helix stability (Table S1). It has also been postulated that the formation of a correctly folded P2 stem inhibits the formation of alternative incorrectly folded structures for the *pbuE* A-riboswitch (32).

The ability of the mutant M6′′ to control eGFP expression over its increased dynamic range was further tested by varying the concentration of ammeline **3** from 0.5–500 μM. From this it can be seen that M6′′ permits excellent dose-dependent control of eGFP expression down to 5.0 μM (Fig. 2*D*). Additionally, the excellent orthogonality with respect to adenine, observed for the M6 mutant, was conserved within both the M6′ and M6′′ riboswitches. To corroborate these observations, the same mutations were introduced into the P2 stem of the mutant M6C riboswitch to give mutants M6C′ (G42A, U47C, U51C, U74C) and M6C′′ (U28G, G42C, U47C, U51C, U74C) (SI Text) (Fig. 1*A*). This also resulted in no change to the observed induction factors of *ca.* 3 for M6C, M6C′, and M6C′′ with both ammeline **3** and azacytosine **4** (Fig. 2*C*). However, as predicted the absolute maximum eGFP production levels increased significantly with an increase in P2 stem strength. Indeed, eGFP production levels for M6C′′ with either ammeline **3** (15.5×10^6 fu/OD) or azacytosine **4** (14.1×10^6 fu/OD) at 500 μM exceed the maximum expression limit of 10.4×10^6 fu/OD for the parental riboswitch in the presence of adenine at 500 μM (Fig. 2*B* and *C*). It was also observed that the M6C′′ displays excellent orthogonal selectivity toward both ammeline **3** and azacytosine **4**, with adenine **1** and guanine **5** again exhibiting little or no induction of eGFP expression (Fig. S3). However, it was noted that guanosine (rG) and 2′-deoxyguanosine (dG) do elicit 1.9- and 2.5-fold induction of eGFP expression, respectively (Fig. S4). This may be due to some similarity between the aptamer domains of M6C′′ and the natural dG-responsive riboswitch from *Mesoplasma florum* (33). These findings above demonstrate that rational modifications of base pairs peripheral to the ligand binding site, which alter the P2 stem strength, allow the expressional landscape to be tuned, resulting in riboswitches that induce low (M6 and M6C), medium (M6′ and M6C′), or high (M6′′ and M6C′′) protein production in response to various nonnatural ligands (Fig. 2*B* and *C*).

New Mutant Riboswitch Pairings Display in Vitro Binding Orthogonality. To probe the ligand–RNA interactions, we produced the aptamer domains (13–83 nt) of the mutant and parental riboswitches by in vitro transcription and studied ligand binding with isothermal titration calorimetry (ITC). In line with the expression results, orthogonal binding selectivity was observed for the aptamer domain of the M6′′ riboswitch, which binds ammeline **3** with an equilibrium dissociation constant (K_d) of 1.19 μM (Fig. 3*A* and *E*), whereas no evidence of binding was observed with the M6′′ aptamer and adenine **1** (Fig. 3*B*). The parental *add* A-aptamer domain bound to adenine **1** with an affinity similar to previous reports (21) and showed no observable binding to

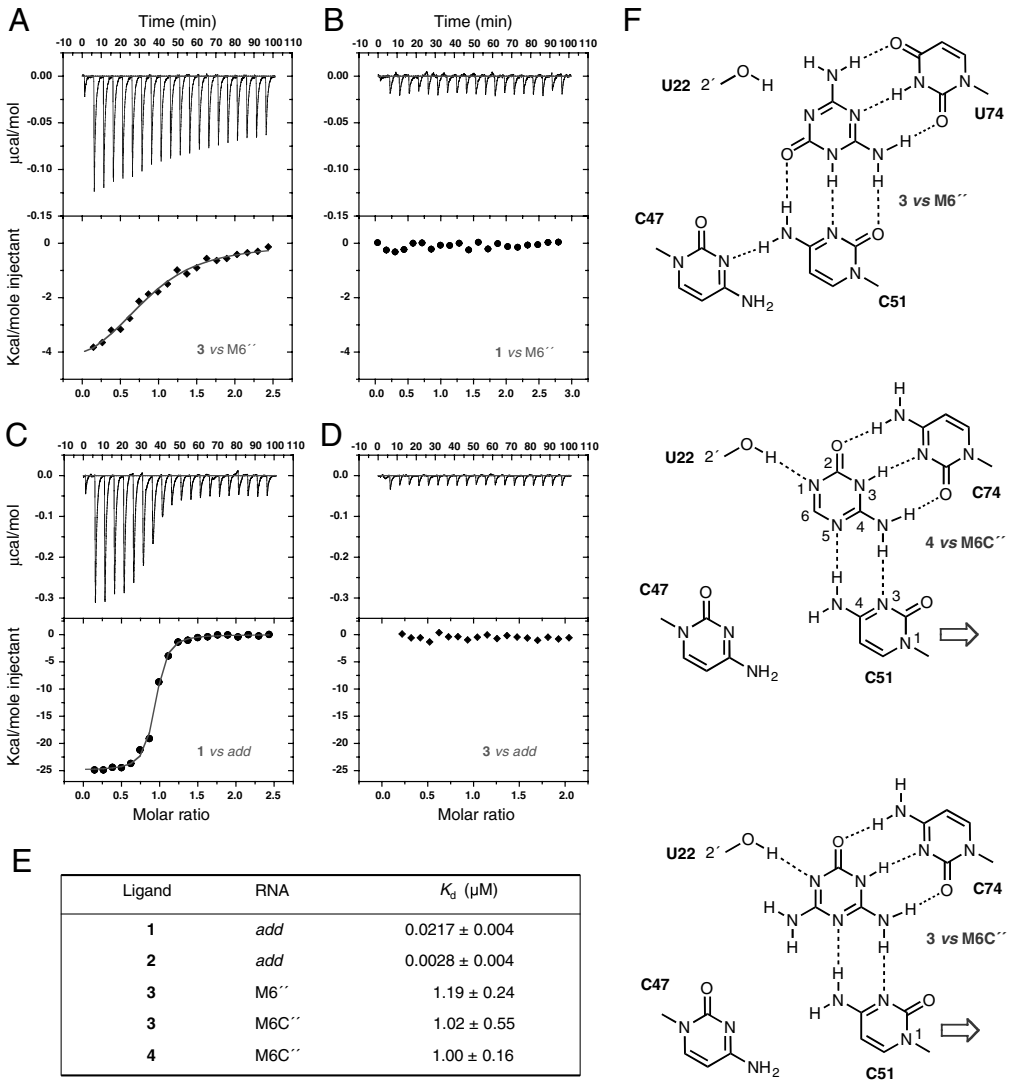

E

Ligand	RNA	K_d (µM)
1	*add*	0.0217 ± 0.004
2	*add*	0.0028 ± 0.004
3	M6′′	1.19 ± 0.24
3	M6C′′	1.02 ± 0.55
4	M6C′′	1.00 ± 0.16

Fig. 3. ITC data and binding site models. (*A*) ITC for ammeline **3** (diamond) versus M6′′ aptamer domain. (*B*) ITC for adenine **1** (circle) versus M6′′ aptamer domain. (*C*) ITC for adenine **1** (circle) versus *add* aptamer domain. (*D*) ITC for ammeline **3** (diamond) versus *add* aptamer domain. (*E*) Dissociation constants (K_d) from ITC (for thermodynamic parameters see Table S2). (*F*) Binding site model for ammeline **3** binding to the M6′′ aptamer domain. Although we propose that C47 makes no direct contact to the ligand, it can be deemed important as it can hydrogen bond to C51, in our mutants, in a similar way that U47 can hydrogen bond to U51 in the wild-type purine riboswitches, which may be important for maintaining the hydrogen bonding network of the J2/3 loop (18, SI Text). This is consistent with the lack of ligand-dependent eGFP induction observed under control of the riboswitches possessing U47C or U51C single point mutations. Also shown is the binding site models for ammeline **3** and azacytosine **4** binding to the M6C′′ (see Fig. 4).

ammeline **3** (Fig. 3*C* and *D*). These results can be rationalized through the binding of ammeline **3**, in its keto tautomeric form, which is able to make six hydrogen bonding contacts with the M6′′ aptamer (Fig. 3*F*) through Watson–Crick–like pairing with U74 and three further constructive hydrogen bond contacts to C51. This mode of binding would be consistent with the binding models proposed for purine riboswitches (18, 21, 23, 24, 34). ITC measurements (Fig. 3*E*) also reveal that ammeline **3** and azacytosine **4** bind to the M6C′′ aptamer domain with K_d values of 1.02 and 1.00 µM, respectively.

Although the ITC results (Fig. 3) are consistent with the observed in vivo orthogonal selectivity, it is apparent that the mutant riboswitches have lower affinities (K_d 1–1.2 µM range) for the selected ligands than the wild-type purine riboswitches, which exhibit K_d values in the low- to mid-nM range with their cognate purine ligands (21). There is thus room for improving the affinities and potentially the in vivo induction factors, either by more extensive mutagenesis remote from the ligand binding site or by rational design of new ligands based upon the azacytosine **4** structural framework. In agreement with previous studies, the binding of adenine **1** and diaminopurine **2** to the parental riboswitch aptamer domain is highly entropically unfavorable and is driven entirely by enthalpy (21) (Table S2). In contrast, the binding of ammeline **3** to mutant riboswitches M6′′ and M6C′′ aptamer domains is both enthalpically and entropically favorable, whereas binding of azacytozine **4** to M6C′′ aptamer domain is largely entropically driven (Table S2).

Crystal Structure of the M6C′′ Aptamer in Complex with 4. Given the structural similarity between ammeline **3** and azacytosine **4**, it is perhaps not surprising that both exhibit similar binding affinity for the M6C′′ aptamer domain. However, unlike the proposed binding mode of ammeline **3** with M6′′ (Fig. 3*F*), the interaction of ligands **3** and **4** with M6C′′ would require a significant change in structure of the ligand binding pocket within the aptamer domain to avoid unfavorable clashes. To explore this, the M6C′′ aptamer (13–83 nt) complexed to azacytosine **4** was crystallized, under conditions similar to those used for the wild-type *add*

A-aptamer-adenine complex (18, SI Text), and the structure was solved to 1.7 Å (Fig. 4*A*) using the molecular replacement method with the *add* A structure (1Y26) (rmsd 1.1 Å) (Table S3). Azacytosine **4** could be clearly identified in the electron density and binds through a Watson–Crick–like base pairing to C74. Further H-bonding is observed to C51 between N5(**4**) and N4(C51) as well as between N4(**4**) and N3(C51) (Figs. 4*B* and 3*F*). An additional H-bond is also made between the 2′OH of U22 and N1 of ligand **4** (Fig. S5). To accommodate these key interactions, several changes in the architecture of the ligand binding site can be observed with respect to the *add* A structure. Firstly, azacytosine **4** appears to be shifted with respect to adenine **1**, causing the C74 to shift toward the major groove (Fig. 4*C*). Additionally, the backbone of the J2/3 loop appears to allow lateral movement of C51 away from C47, by 1.8 Å, toward the central core of the ligand binding site. Lateral movement of C51 has previously been observed within a U51C mutant riboswitch that recognises 2′-deoxyguanosine (33). Unlike the previous studies, however, the nucleotide at position 47 in the present structure is not dramatically perturbed and does not point away into the solvent phase (Fig. 4*C*). Finally, coordination to Mg^{2+} is also shown to induce a kink in the phosphodiester backbone between U22 and A23, enabling the 2′OH of U22 to engage with N1 lone pair of **4** (Fig. S5).

Conclusions

Using a combination of chemical genetics and genetic selection a riboswitch double mutant (M6) was selected from a total pool of close to 1200 riboswitch–ligand pairings. Notably, this mutant and the related triple mutant (M6C) control in vivo gene expression in response to nonnatural ligands ammeline **3** or azacytosine **4**, respectively, in a precise dose-dependent fashion. These riboswitches display excellent orthogonal selectivity with respect to the parent riboswitch. Thus, M6 and M6C do not respond to adenine or guanine, nor does the parent riboswitch interact with ammeline **3** or azacytosine **4**. Furthermore, by introducing mutations into the P2 stem, remote from the ligand binding site, it was shown to be possible to fine-tune the accessible gene expression landscape, providing riboswitches (M6′′ and M6C′′) that cover a broad dynamic range of gene expression levels. ITC binding studies were also used to confirm the orthogonal selectivity of the mutant and parent riboswitches in vitro. Finally, the x-ray crystal structure of the orthogonal riboswitch M6C′′ demonstrates the inherent flexibility of the ligand binding site.

Taken together the results presented here form the basis for an approach to reengineer natural riboswitches, providing new genetic switches that allow dose-dependent, orthogonally selective, and dynamic control of gene expression and further exemplify the functional and structural versatility of RNA. Reengineered riboswitches are potentially useful orthogonal components for synthetic biology and could also find application for gene functional analysis in vivo, where simultaneous differential control of multiple genes would be desirable.

Materials and Methods

Construct Design, Selection, and Reporter Assay. A synthetic construct containing the *lac* promoter/operator upstream of the *add* A-riboswitch from *Vibrio vulnificus* (4, 18), optimized to give an improved induction factor within *E. coli*, was purchased (Yorkshire Bioscience) and subcloned with *Eco*RI and *Hind*III into the pMOD3 vector. The CAT selection gene and eGFP reporter gene were PCR amplified, digested using *Eco*RV and *Not*I, and ligated into the pMOD3 vector, which had been digested with *Nco*I, Klenow filled, then digested with *Not*I to give CAT and eGFP parental vectors (SI Text Fig. S1).

Mutants M1–15 were introduced into the CAT vector template, using the multi-site-directed mutagenesis kit (Stratagene). The resulting plasmids were used to transform *E. coli*, and single colonies were picked and checked by sequencing. Mutants were initially screened on LB agar plates containing 170 μg/ml chloramphenicol, 1 mM IPTG, and 250 μM ligand from the library of 80 ligands (Fig. S2). Colonies that survived in the presence of a particular

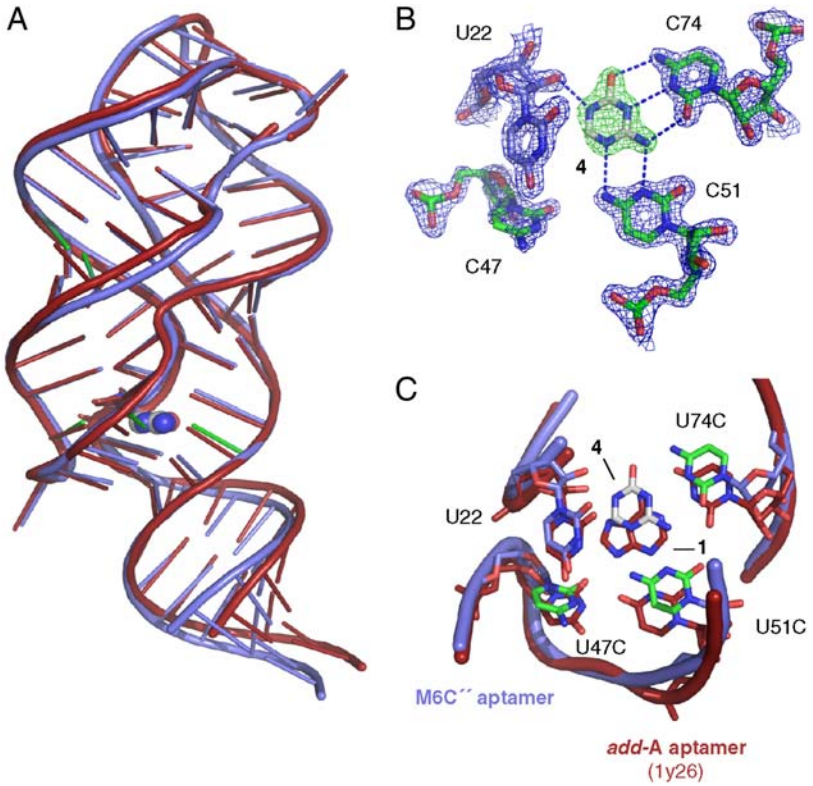

Fig. 4. Crystal structure of mutant M6C′′ bound to ligand **4**. (*A*) M6C′′ (*Blue*) overlayed with the *add A* (*Red*). Mutated residues are shown in green. (*B*) Azacytosine **4** bound to the M6C′′ displayed with mF_o-DF_c sigma a-weighted omit map, contoured at 3.5σ. (*C*) Overlay of ligand binding sites of *add* A (*Red*), and M6C′′ (*Blue*).

ligand, were selected for further characterization. Growth assays were conducted using cells grown overnight in LB at 37 °C, which were diluted 1/20 into fresh M9 medium containing 1 mM IPTG, and then grown at 37 °C for 1 h. 170 μg/ml Chloramphenicol and 500 μM of the selected ligand were added, and bacterial cell growth was monitored by UV absorbance at 620 nm using an Anthos Zenyth 3100 plate reader.

The mutants identified from the CAT selection were cloned into the eGFP parental vector (using *Bam*HI and *Bbs*I restriction sites) and sequenced. The U74C mutation was introduced into the M6-eGFP expression vector via site-directed mutagenesis to afford the M6C-eGFP construct. The P2 stem mutants, G42A (′) and U28G, G42C (″), were again produced by site-directed mutagenesis and checked by sequencing. Expression assays were conducted using cells grown overnight in LB at 37 °C, which were diluted 1/20 into fresh M9 medium with 1 mM IPTG and grown at 37 °C for 1 h. The selected ligand (5 mM DMSO stock) was added, and fluorescence intensity units (using $485_{ex}/535_{em}$ filters) normalized for cell density (620_{abs} filter) were measured using the Anthos Zenyth 3100 plate reader.

In Vitro RNA Production, ITC, and X-Ray Crystallography. In vitro transcribed RNA (aptamer domains 13–83 nt) of identical length to that used in previous studies (18, 21), were prepared from double-strand DNA templates, using standard procedures (SI Text). The transcripts were then purified under native conditions by size exclusion chromatography, and assessed for purity under denaturing conditions (8.0 M Urea, 12% polyacrylamide gel).

RNA samples for ITC, were exhaustively dialyzed overnight at 4 °C against 50 mM K HEPES pH 7.5, 20 mM $MgCl_2$, 100 mM KCl and degassed. ITC was performed with the concentration of the injectant 10 times higher than the cell concentration. Experiments were performed at 25 °C using a VP-ITC microcalorimeter (Microcal, Inc) with 20 injections of 15.0 μL with a reference power of 2.0 kcal/s.

For crystallography, the purified M6C″-**4** complex was prepared at 0.52 mM in 50 mM K HEPES buffer pH 7.5, 5.0 mM $MgCl_2$, 100 mM KCl and cocrystallized under conditions similar to those previously described (18). Diffraction data (Table S3) were collected at DLS, Oxfordshire. Coordinates and structure factors have been deposited into the Protein Data Bank (PDB access code 3LA5).

ACKNOWLEDGMENTS. This work was supported by the Biotechnology and Biological Sciences Research Council through the Selective Chemical Intervention in Biological Systems Initiative (Grant BB/D005612/1) and a PhD studentship award for J.N.D. We also thank Sri A. Lestari for technical support and Dr. Graeme L. Conn for helpful advice.

1. Vitreschak AG, Rodionov DA, Mironov AA, Gelfand MS (2004) Riboswitches: The oldest mechanism for the regulation of gene expression. *Trends Genet*, 20:44–49.
2. Sudarsan N, Barrick JE, Breaker RR (2003) Metabolite-binding RNA domains are present in the genes of eukaryotes. *RNA*, 9:644–647.
3. Barrick JE, Breaker RR (2007) The distributions, mechanisms, and structures of metabolite-binding riboswitches. *Genome Biol*, 8:R239.
4. Mandal M, Breaker RR (2004) Adenine riboswitches and gene activation by disruption of a transcription terminator. *Nat Struct Mol Biol*, 11:29–35.
5. Coppins RL, Hall KB, Groisman EA (2007) The intricate world of riboswitches. *Curr Opin Microbiol*, 10:176–181.
6. Winkler WC, Nahvi A, Roth A, Collins JA, Breaker RR (2004) Control of gene expression by a natural metabolite-responsive ribozyme. *Nature*, 428:281–286.
7. Cheah MT, Wachter A, Sudarsan N, Breaker RR (2007) Control of alternative RNA splicing and gene expression by eukaryotic riboswitches. *Nature*, 447:497–501.
8. Link KH, Breaker RR (2009) Engineering ligand-responsive gene-control elements: Lessons learned from natural riboswitches. *Gene Ther* 1–13.
9. Werstuck G, Green MR (1998) Controlling gene expression in living cells through small molecule-RNA Interactions. *Science*, 282:296–298.
10. Lynch SA, Desai SK, Sajja HK, Gallivan JP (2007) A High-throughput screen for synthetic riboswitches reveals mechanistic insights into their function. *Chem Biol*, 14:173–184.
11. Fowler CC, Brown ED, Li Y (2008) A FACS-based approach to engineering artificial riboswitches. *ChemBioChem*, 9:1906–1911.
12. Weigand JE, et al. (2008) Screening for engineered neomycin riboswitches that control translation initiation. *RNA*, 14:89–97.
13. Kim D-S, Gusti V, Pillai SG, Gaur RK (2005) An artificial riboswitch for controlling pre-mRNA splicing. *RNA*, 11:1667–1677.
14. Weigand JE, Suess B (2007) Tetracycline aptamer-controlled regulation of pre-mRNA splicing in yeast. *Nucleic Acids Res*, 35:4179–4185.
15. Wieland M, Hartig JS (2008) Improved aptazyme design and in vivo screening enable riboswitching in bacteria. *Angew Chem Int Ed*, 47:2604–2607.
16. Ogawa A, Maeda M (2008) An artificial aptazyme-based riboswitch and its cascading system in *E. coli*. *ChemBioChem*, 9:206–209.
17. Nomura Y, Yokobayashi Y (2007) Re-engineering a natural riboswitch by dual genetic selection. *J Am Chem Soc*, 129:13814–13815.
18. Serganov A, et al. (2004) Structural basis for discriminative regulation of gene expression by adenine- and guanine-sensing mRNAs. *Chem Biol*, 11:1729–1741.
19. Rieder R, Lang K, Graber D, Micura R (2007) Ligand-induced folding of the adenosine deaminase a-riboswitch and implications on riboswitch translational control. *ChemBioChem*, 8:896–902.
20. Gilbert SD, Reyes FE, Edwards AL, Batey RT (2009) Adaptive ligand binding by the purine riboswitch in the recognition of guanine and adenine analogs. *Structure*, 17:857–868.
21. Gilbert SD, Mediatore SJ, Batey RT (2006) Modified pyrimidines specifically bind the purine riboswitch. *J Am Chem Soc*, 128:14214–14215.
22. Mandal M, Breaker RR (2004) Gene regulation by riboswitches. *Nat Rev Mol Cell Biol*, 5:451–463.
23. Wickiser JK, Cheah MT, Breaker RR, Crothers DM (2005) The kinetics of ligand binding by an adenine-sensing riboswitch. *Biochemistry*, 44:13404–13414.
24. Lemay J-F, Penedo JC, Tremblay R, Lilley DMJ, Lafontaine DA (2006) Folding of the adenine riboswitch. *Chem Biol*, 13:857–868.
25. Gilbert SD, Stoddard CD, Wise SJ, Batey RT (2006) Thermodynamic and kinetic characterization of ligand binding to the purine riboswitch aptamer domain. *J Mol Biol*, 359:754–768.
26. Roth A, Breaker RR (2009) The structural and functional diversity of metabolite-binding riboswitches. *Annu Rev Biochem*, 78:305–334.
27. Ottink OM, et al. (2007) Ligand-induced folding of the guanine-sensing riboswitch is controlled by a combined predetermined-induced fit mechanism. *RNA*, 13:2202–2212.
28. Batey RT, Gilbert SD, Montange RK (2004) Structure of a natural guanine responsive riboswitch complexed with the metabolite hypoxanthine. *Nature*, 432:411–415.
29. Zuker M (2003) Mfold web server for nucleic acid folding and hybridization prediction. *Nucleic Acids Res*, 31:3406–3415.
30. Thirumalai D, Hyeon C (2005) RNA and protein folding: Common themes and variations. *Biochemistry*, 44:4957–4970.
31. Lin JC, Thirumalai D (2008) Relative stability of helices determines the folding landscape of adenine riboswitch aptamers. *J Am Chem Soc*, 130:14080–14081.
32. Greenleaf WJ, Frieda KL, Foster DAN, Woodside MT, Block SM (2008) Direct observation of hierarchical folding in single riboswitch aptamers. *Science*, 319:630–633.
33. Edwards AL, Batey RT (2009) A structural basis for the recognition of 2′-deoxyguanosine by the purine riboswitch. *J Mol Biol*, 385:938–948.
34. Noeske J, Schwalbe H, Wöhnert J (2007) Metal-ion binding and metal-ion induced folding of the adenine-sensing riboswitch aptamer domain. *Nucleic Acids Res*, 35:5262–5273.